Polymer assisted deposition of YIG thin films with thickness control for spintronics applications

View Online　　Export Citation　　CrossMark

Rubén Corcuera,[1,2] (iD)　Pilar Jiménez-Cavero,[3,a)] (iD)　Rafael Pérez del Real,[4] (iD)　Francisco Rivadulla,[5,6] (iD)
Rafael Ramos,[5,6] (iD)　José Ignacio Morales-Aragonés,[1,2] (iD)　Soraya Sangiao,[1,2] (iD)　César Magén,[1,2] (iD)
Luis Morellón,[1,2] (iD)　and Irene Lucas[1,2] (iD)

AFFILIATIONS

[1] Instituto de Nanociencia y Materiales de Aragón, Universidad de Zaragoza-CSIC, 50018 Zaragoza, Spain
[2] Departamento de Física de la Materia Condensada, Universidad de Zaragoza, 50009 Zaragoza, Spain
[3] Centro Universitario de la Defensa, Academia General Militar, 50090 Zaragoza, Spain
[4] Instituto de Ciencia de Materiales de Madrid-CSIC, 28049 Madrid, Spain
[5] Centro Singular de Investigación en Química Biolóxica e Materiais Moleculares (CIQUS), Universidade de Santiago de Compostela, 15782 Santiago de Compostela, Spain
[6] Departamento de Química-Física, Universidade de Santiago de Compostela, 15782 Santiago de Compostela, Spain

[a)] Author to whom correspondence should be addressed: pjcavero@unizar.es

ABSTRACT

The use of magnetic garnets in new technologies such as spintronic devices requires fine-structured thin films. Classical fabrication techniques for these materials, typically physical vapor deposition methods, lead to excellent magnetic behavior. However, availability and scalability for potential applications are well restricted. In this study, we propose an innovative approach to fabricating Yttrium Iron Garnet thin films with precise thickness control achieved through iterative layer deposition via a chemical synthesis route. Remarkably, the iterative deposition process results in films exhibiting exceptional crystallinity. Magnetic characterization provides saturation magnetization and coercivity values on par with those reported in literature, summed to narrow ferromagnetic resonance lines. Therefore, in this work we demonstrate the viability of polymer assisted deposition as a promising alternative thinking about scalability to conventional deposition techniques for this material. Notably, our findings reveal energy conversion efficiencies comparable to those achieved with materials synthesized via physical vapor deposition methods.

I. INTRODUCTION

The development of spintronics, magnonics, and spin caloritronics in recent years has led to a renewal of interest in the family of magnetic garnets due to their exceptional magneto-optical properties.[1–6] In particular, the net magnetic moment combined with insulating behavior, small spin-wave damping leading to narrow ferromagnetic resonance (FMR) linewidth, and optical transparency in a wide range are of special relevance for these fields.[7]

Among the materials belonging to this family, FMR linewidth and damping parameter reach their minimum in bulk single crystals of $Y_3Fe_5O_{12}$ (YIG), with peak-to-peak and Gilbert damping values of 0.5 mOe and 10^{-5}, respectively.[8,9] When fabricating YIG thin films, these FMR linewidth and damping values worsen in, at least, an order of magnitude, depending on the fabrication technique.[1,7,10–12] These facts make it an outstanding synthetic material for microwave and magneto-optical applications such as filters and resonators, and has established YIG as the benchmark material for the study of novel spintronic phenomena.

YIG is a cubic iron garnet ($Ia\bar{3}d$, O_h^{10}, space group 230) where the Fe^{3+} ions occupy different octahedral:tetrahedral sites in the ratio 2:3. The Fe^{3+} sublattices order antiferromagnetically, with non-magnetic Y^{3+} ions located at the dodecahedral sites. Therefore, it is the uncompensated Fe^{3+} ions at the tetrahedral sites that are responsible for the ferrimagnetic state at room temperature, up to a Curie temperature ~560 K.[13,14]

In the aforementioned fields, the availability of epitaxial thin films is essential for most studies and applications. However, the standard method for YIG single-crystal fabrication, liquid phase epitaxy (LPE),[7] and other bulk synthetic methods have difficulties in controlling the layer thickness down to the nanometer range,[15] although successful attempts have been achieved recently with really good FMR linewidth and damping values.[16–18] On the other hand, physical techniques such as pulsed laser deposition (PLD) or sputtering produce high-quality epitaxial thin films of YIG of a few nanometers with low values of magnetization damping[6,11,19–24] but show important drawbacks in terms of affordability and scalability compared to chemical synthesis routes.[25] In this regard, we reported in a previous study[26] the possibility of fabricating epitaxial YIG thin films on (111)-oriented $Gd_3Ga_5O_{12}$ (GGG) substrates using a scalable and reliable chemical solution (water-based) deposition technique called polymer assisted deposition (PAD). The obtained samples retained chemical, crystalline, and magnetic properties comparable to those of films produced by physical methods. Structural and chemical properties as well as static and dynamic magnetic behavior of ~15 nm thick films were studied in that work. In particular, the magnetization saturation M_S and the Gilbert damping α values were determined by broadband FMR experiments.

Some spintronic applications require samples of tens of nanometers of thickness for improved performance; that is the case of the longitudinal spin-Seebeck effect (LSSE).[27–29] This phenomenon consists of the excitation of a spin current in a magnetically ordered material (FM) as a consequence of the application of a thermal gradient. The consensus at present is that the heat-driven spin current refers to that transported by the collective excitations of local moments (magnons).[30–32] Therefore, electrical insulators are the most suitable materials for the magnetically active layer.[33] Detection is usually performed by spin-to-charge conversion: the thermally excited spin current is injected into an adjacent non-magnetic (NM) material, where it is converted into a transverse electric field by means of the inverse spin-Hall effect (ISHE).[34] The longitudinal spin Seebeck effect is the simplest configuration in which a bulk polycrystalline ferromagnet can be used and considered as a prototype of the spin Seebeck effect from an application viewpoint.[35]

The finite magnon propagation length inside the FM layer leads to a saturating behavior of the signal upon increasing the layer thickness. In the case of YIG fabricated by PLD, this length scale is around ~100 nm at room temperature.[27] Another factor with great impact in the observation of the LSSE is the interface quality since it affects interfacial properties such as spin-mixing conductance, sd-exchange coupling, or interfacial thermal resistivity.[27]

In this work, we show that the PAD technique is a suitable technique to fabricate YIG thin films with thickness control and interface quality, obtaining excellent crystalline and magnetic (static and dynamic) properties. Furthermore, the LSSE is quantified as a function of the thickness of the films.

II. EXPERIMENTAL

Fabrication of the samples was made by means of PAD. Individual Y and Fe solutions were prepared by dissolving their nitrates in water with ethylenediaminetetraacetic acid (EDTA, 1:1 molar ratio) and polyethylenimine (PEI) (1:1 mass ratio to EDTA). Each individual solution was filtrated using Amicon filtration units (10 kDalton). Eventually, the yttrium-iron solution was made by mixing the individual solutions in the ratio of 3 mol of yttrium to 5 mol of iron. 70 μl of the solution were spin-coated onto GGG (111) polished substrates using a Spin Coater WS-650MZ-23NPPB from Laurell. The crystallization process was performed in air using a Hobersal Mod. 12 PR/200 oven at 750 °C during 2 h with well-controlled thermal ramps to avoid cracking of the films. Thickness control of the films was achieved with an iterative process of spin-coating and crystallization in the oven.

The samples were structurally characterized by x-ray reflectivity (XRR) and diffraction (XRD) in a high-resolution Bruker D8 Advance diffractometer using Cu $K_{\alpha 1}$ radiation. The reflectivity profiles were analyzed using a commercial software provided by Bruker. Local structure characterization was carried out by scanning transmission electron microscopy STEM in a probe-corrected Thermo Fisher Scientific Titan 60–300 microscope, equipped with a CETCOR aberration corrector for the condenser system to achieve a probe size <1 Å. Cross-sectional thin lamellas (<50 nm thick) were extracted from the films for STEM characterization by focused-ion-beam (FIB) milling in a Thermo Fisher Scientific Helios Nanolab 600 operated at 30 kV. A 5-kV ion beam was used for the final thinning to reduce the surface amorphization layer. The morphology of the surface of samples was studied by Atomic Force Microscopy in tapping mode using a Veeco (Bruker) Multimode VIII system.

Static magnetic properties of the samples were investigated using a Vibrating Sample Magnetometer (VSM) KLATencorEV7a to extract saturation magnetization and coercivity. Magnetic dynamic properties were studied through temperature dependent ferromagnetic resonance using a Bruker EMX spectrometer operating at 9.4 GHz (X band), equipped with an ER 4102ST resonant cavity (TE102 mode) for low magnetic fields. Broadband FMR measurements were carried out at room temperature on YIG samples flipped upside down on a shorted microstrip line placed between the poles of an electromagnet that provides static magnetic fields up to 1 T in the plane of the samples and perpendicular to the rf field. Excitation frequencies of the rf magnetic field in the range from 2 to 7 GHz at a power of 10 dBm have been selected using a Keysight N5173B rf generator. The FMR signal was measured by a lock-in technique with an amplitude modulation at a few kHz. Additionally, time-dependence response to transverse magnetic pulses and low bias fields has been investigated using a pulsed inductive microwave magnetometer (PIMM).[36]

In order to achieve ISHE detection of the LSSE, a Pt layer of ~5.5 nm was deposited by dc magnetron sputtering at room temperature and an Ar pressure of 0.5 mTorr prior to LSSE experiments. The sample was then cut into 2 × 10 mm^2 sized pieces. Finally, the used experimental setup for the LSSE study consists of a copper holder in which the sample is placed between two AlN plates attached to the holder; the thermal gradient in the direction perpendicular to the sample surface (z direction) is generated by the application of an electric current to a resistive heater placed on the

upper plate using a Keithley 236 source. The temperature difference between plates is monitored by two T-type thermocouples connected to a Keithley 2000 multimeter. The electrical contacts were made using Al wires with 25 μm diameter, and the output transverse voltage along the 10 mm-long side (y direction) is recorded using a Keithley 2182A nanovoltmeter. The sample is placed between the pole pieces of an electromagnet powered by a TDK Lambda power supply, achieving up to 1 T field, with the field applied in-plane parallel to the 2 mm-long side (x direction).

III. RESULTS AND DISCUSSION

A. Structural characterization

The main limitation of the PAD technique is the obtained thickness in a single deposition that depends typically on the viscosity of the solution and that normally ranges from 12–20 nm. For thicker samples, the deposition process must be repeated, with the possibility of damaging the previous crystallized layer. In this work, a layer-on-layer growth was used, where a new layer was stacked onto a previous thinner sample by spin-coating followed by an annealing process to induce further crystallization. Therefore, the evolution of the crystallinity of the material with the increased number of stacked layers in six different samples has been studied and carefully analyzed.

XRD $2\theta/\omega$ patterns around the GGG (444) peak confirm the crystalline growth of YIG in each stacked deposition, as shown in Fig. 1(a). Laue fringes can be observed, which entails high crystal coherence within the film. Furthermore, diffraction patterns do not exhibit any other peaks but (hhh) ones in the 2θ 20°–120° range (see supplementary material). The final thicknesses of the samples after each intermediate deposition were assessed by fitting the XRR data, as shown in Fig. 1(b) for a two layer-stacked sample. According to the fits, the thickness of each stacked layer for all the samples was

around 12.5 nm with a surface roughness of $\simeq$ 0.3 nm (a detail of the sample properties can be seen in supplementary material).

The AFM topography image shown in Fig. 2(a) reveals a homogeneous surface with RMS roughness below 1 nm obtained in a micron-sized region, in agreement with the XRR profiles. High angle annular dark field (HAADF) imaging in STEM was carried out to investigate the local microstructure and the presence of porosity within the films. A low magnification image of a four-layer specimen confirms the low roughness of the film [see Fig. 2(b)]. Furthermore, the thickness of the whole stack can be accurately determined to (55 ± 1 nm). A higher magnification image of the whole film is displayed in Fig. 2(c) showcasing that a high quality single crystal is grown, without any noticeable discontinuity or defect at the interfaces between the stacked layers. Finally, the atomic resolution HAADF STEM image of the interface of the YIG film with the GGG substrate, illustrated in Fig. 2(d), reveals the high quality epitaxy of the film, a coherently strained film with an atomically sharp interface.

B. Magnetic properties

VSM measurements at room temperature reported hysteresis loops. The coercive field of the samples was measured, obtaining similar results as the ones presented in Fig. 3(a) for the 25, 50, and 75 nm thick samples; all the samples exhibited coercive fields smaller than 0.5 Oe, which demonstrates excellent magnetic behavior compared to literature reported samples.[11,16,37] The saturation magnetization of all samples is in the range of $\simeq$140 emu/cm^3, which is the standard value taken for bulk YIG.[38]

FMR experiments reported a single sharp line with ΔH_{pp} values $\simeq$6 G at 9.4 GHz [Fig. 4(a)]. This result is in excellent agreement with recently reported values of monocrystalline thin films like the obtained in Ref. 16, and just 2–3 times larger than in samples fabricated through physical vapor deposition techniques.[23,39] The specimens analyzed were randomly extracted from the sample
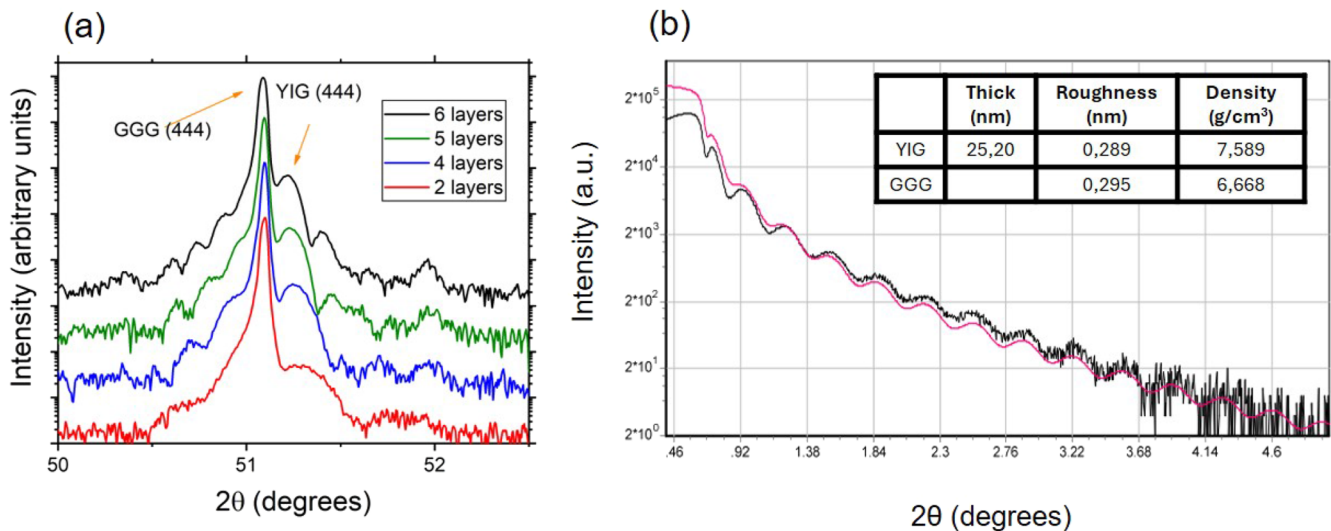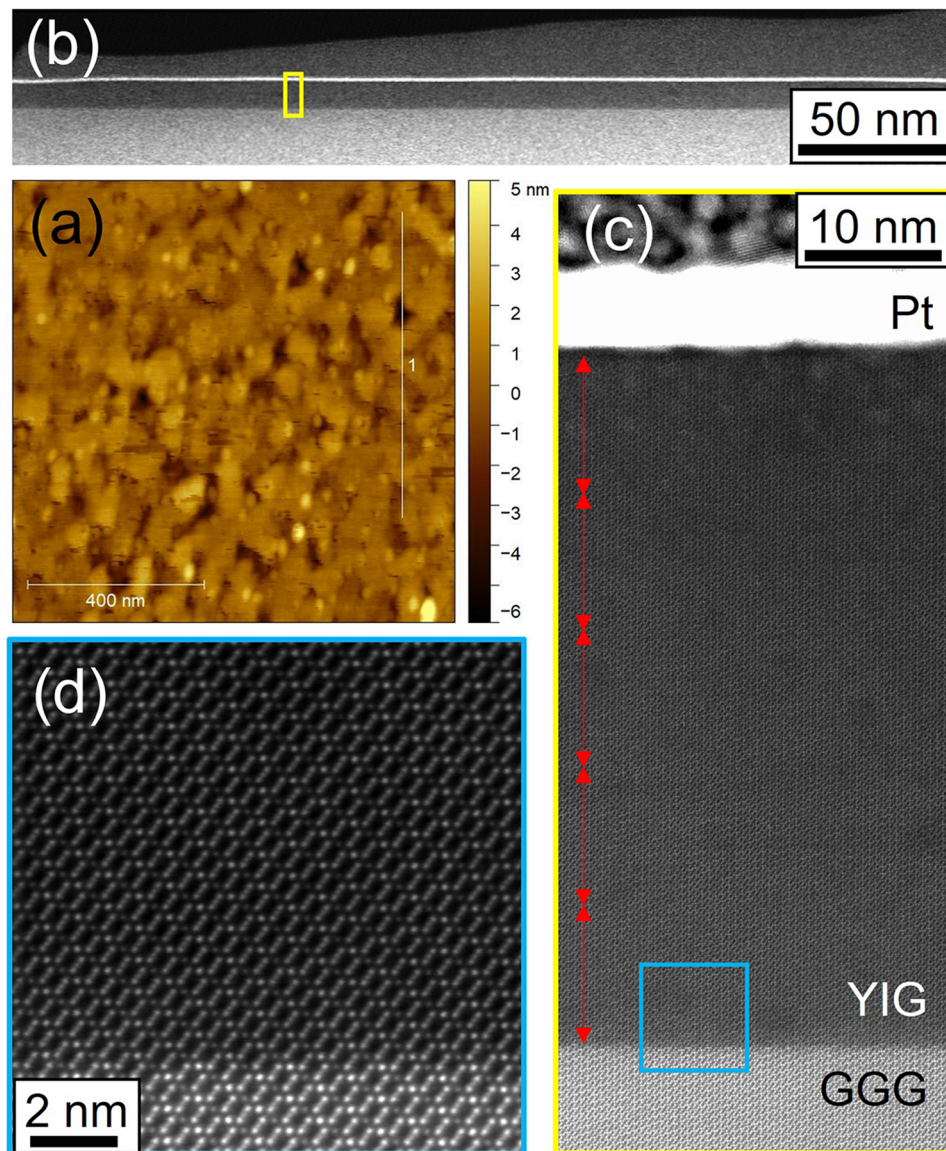
FIG. 1. (a) Symmetric $2\theta/\omega$ diffraction patterns around the (444) GGG Bragg peak after each deposition. (b) XRR data and fit of a two stacked-layer sample.

FIG. 2. (a) AFM topography of the surface (1×1 μm^2) of a 55 nm thick film. (b) Low magnification HAADF-STEM image of a 55 nm thick film. (c) High-resolution image of the whole stack of the 55 nm thick YIG film, approximately from the yellow rectangular region in (b). The red arrows are a guide to the eye schematizing the estimated thickness of each stacked layer. (d) Atomic resolution HAADF-STEM image of the interface between the GGG substrate and YIG film, marked with a blue square in (c).

and reproducible, ensuring magnetic homogeneity throughout the samples.

Resonant frequency dependence of the 75 nm thick film with the applied magnetic field is shown in Fig. 4(b); it can be seen that follows the Kittel formula[40]

$$f = \left(\frac{\gamma}{2\pi}\right)\sqrt{H_r(H_r + 4\pi M_s)}. \tag{1}$$

With the fit of the data to Eq. (1), saturation magnetization M_s and gyromagnetic value γ are extracted. The M_s values obtained are

151 emu/cm^3, which arises just to an 8% discrepancy with the value measured by VSM. This difference may be attributed to the fact that FMR provides an effective value of the saturation magnetization considering the effect of anisotropies present in the sample.[16,41] It is also worth mentioning that the difficulties in measuring the exact volume of the sample yield large values of error in the saturation magnetization.[16] The gyromagnetic value from the fitting is calculated to be $\frac{\gamma}{2\pi} \simeq 2.1$ MHz/Oe. Both results are comparable to bulk YIG ($M_s \simeq 140$ emu/cm^3 and $\gamma/2\pi \simeq 2.8$ MHz/Oe). The Gilbert damping parameter α can be extracted from the linear fit
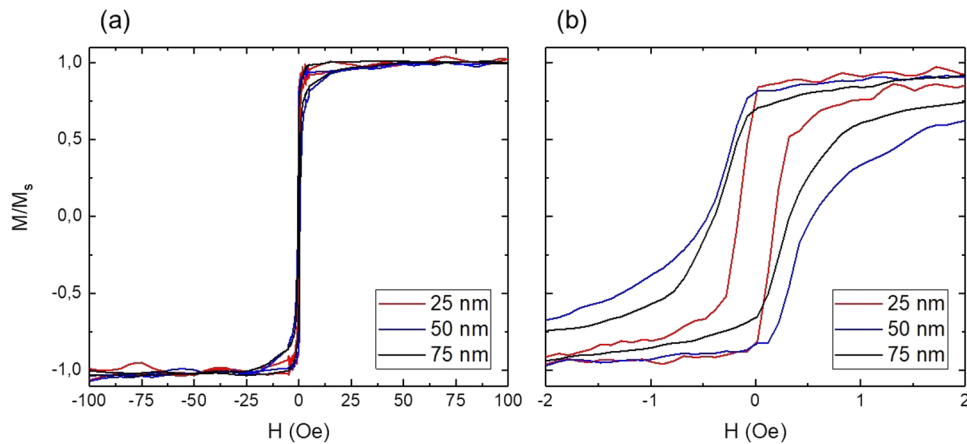
FIG. 3. (a) Normalized hysteresis loops of 2, 4, and 6 stacked-layer samples measured in the film plane. All the measurements exhibit coercive fields lower than 1 Oe and saturation magnetization near 140 emu/cm^3. (b) Hysteresis loops close to the zero field.

to Eq. (2) of the broadening of the FMR peak with increasing frequency,[42,43]

$$\mu_0 \Delta H = \mu_0 \Delta H_0 + \frac{4\pi\alpha}{\gamma} f. \qquad (2)$$

This linear fit [Fig. 4(c)] yields a negative intercept of -0.3 ± 4.9 Oe, but its value is much smaller than its standard error, which means that the value of this inhomogeneous linewidth broadening is approximately zero. The slope of the linear fit yields to $\alpha \simeq 8.9 \times 10^{-3}$. This value is two orders of magnitude larger when compared to bulk material[9] and an order of magnitude larger compared to monocrystalline thin films fabricated via physical routes[23,24,39] and alternative chemical routes.[15,16]

Figure 5(a) shows the PIMM inductive response voltage for a bias magnetic field of 40 Oe applied to the 75 nm thick sample in the film plane. From these PIMM measurements, for all thicknesses and for bias fields applied between 5 and 90 Oe, the resonance frequencies shown in Fig. 5(b) have been obtained. The resonance

frequency is the same for all thicknesses, which proves the quality and homogeneity of the samples. Besides, those values fit perfectly with the fit shown in Fig. 4(b), obtained for much higher applied fields and different techniques. Using the Fast Fourier transform (FFT) of Fig. 5(a), taking into account that[44]

$$\alpha = \frac{\Delta\omega}{\gamma\mu_0 M_s}, \qquad (3)$$

where $\Delta\omega$ is the full width at half maximum resonance linewidth, we obtain a value of $\alpha \simeq 10 \times 10^{-3}$, which fits perfectly with the value obtained using the previous technique for higher fields.

C. Spintronics response

The results of the LSSE experiments at $T = 300$ K are presented below. The transverse voltage ΔV_y is recorded for different temperature gradients applied in the z-direction (out-of-plane), while the magnetic field (applied in the x direction) is swept twice (from $H = -8$ kOe to $H = 8$ kOe and back). Taking advantage of the odd
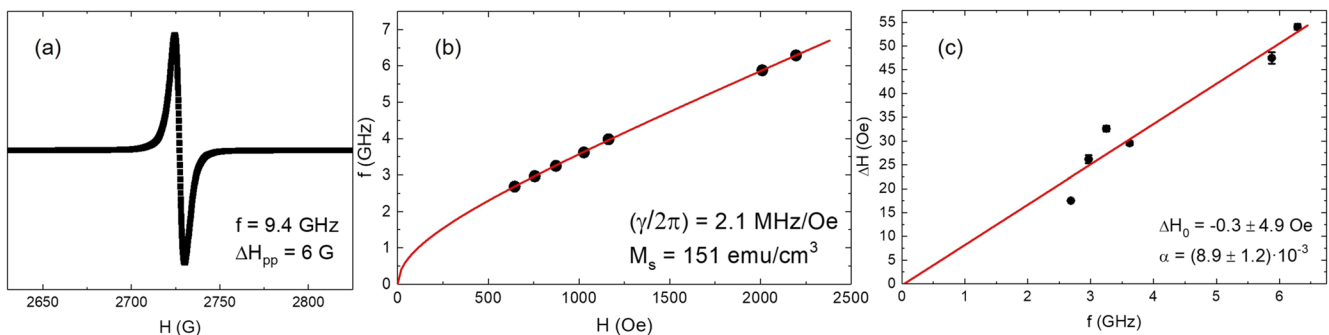
FIG. 4. (a) Ferromagnetic resonance spectrum of the 37 nm thick sample. A single sharp line is obtained with $\Delta H_{pp} = 6$ G at 9.4 GHz. (b) Magnetic field dependence of the resonant frequency of the 75 nm thick film and fitting to the Kittel formula. The measurements were performed with the bias field along the film surface. (c) FMR linewidth broadening vs frequency and linear fit to Eq. (2).
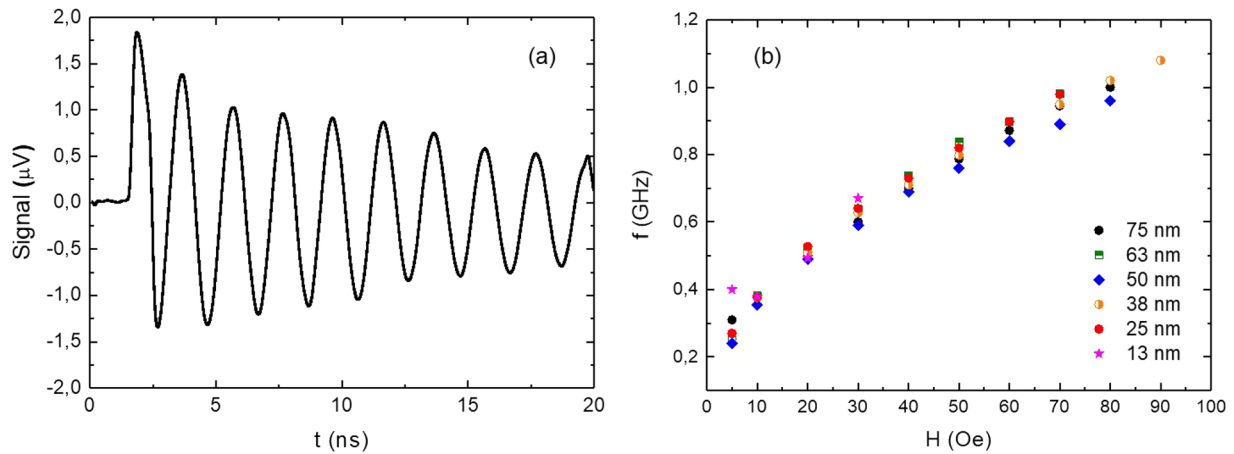
FIG. 5. (a) PIMM inductive response voltage for a bias magnetic field of 40 Oe applied to the 75 nm thick sample along the film plane. (b) FMR obtained for low fields and all the thickness used in this study with this PIMM technique.

parity of the ISHE signal as a function of magnetic field, the antisymmetric component $\Delta V_y^{\text{anti}}(H)$ of the raw data is extracted for each applied ΔT in order to retrieve the ISHE contribution. The resulting signals are plotted in Fig. 6(a). As expected, $\Delta V_y^{\text{anti}}(H)$ mirrors the hysteresis loop of YIG with a coercivity below the field resolution of our measurement. The ΔV_{ISHE} value is then calculated for each ΔT as half the difference between saturated positive and negative ΔV_y^{anti}. The resulting values depend linearly on ΔT, as plotted in Fig. 6(b).

The evolution of the thermal-spin current generation was studied with film thickness. The magnitude of the SSE increases rapidly until 50 nm, where it seems to reach a value that does not increase significantly for thicker samples, as seen in Fig. 6(c).

These values allow to calculate the standard SSE coefficients (S_{zy}^{SSE}) defined as follows:

$$S_{zy}^{\text{SSE}} = \frac{\Delta V_{\text{ISHE}}}{\Delta T} \frac{t}{d_y}, \qquad (4)$$

where t denotes the sample thickness (including substrate) and d_y is the distance between the electrical contacts to measure the signal. We obtain $S_{zy}^{\text{SSE}} = 2.45 \pm 0.05$ nV K^{-1} for the thickest sample. These values are around one or two orders of magnitude smaller than those reported in the literature for bulk and thin films of comparable thickness fabricated using physical vapor deposition techniques.[27,31,45,46] This could be attributed to various causes: minor variations in the Pt layer thickness, for example, affect greatly the ISHE voltage through the spin diffusion length,[47] the Pt/YIG interface or some incidence of porosity could also result in a reduction of the spin transference: a small variation in the surface composition, with a reduced magnetization, could be responsible of this low response as well. This deserves further investigation. Despite the low S_{zy}^{SSE} obtained, the results attained in this work demonstrate the possibility of using a scalable and affordable chemical route to synthesize thin films to be implemented in thermal spintronics applications.
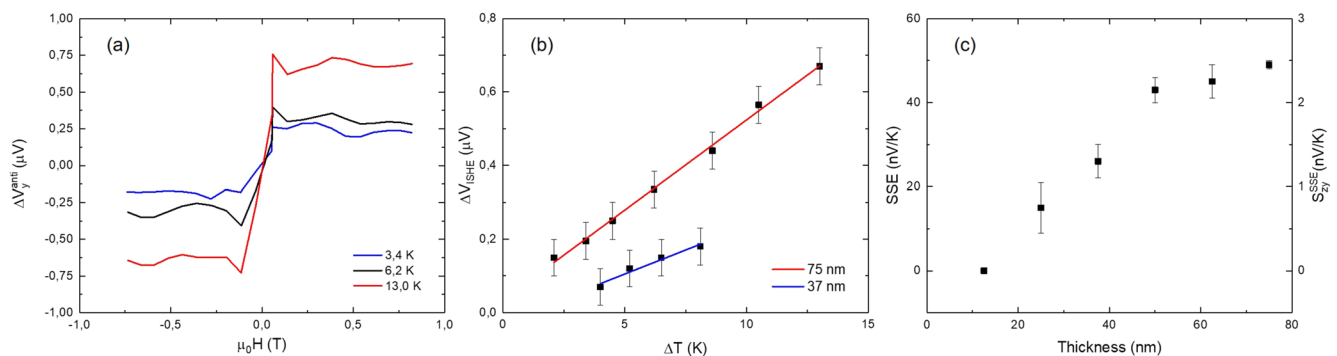
FIG. 6. (a) Antisymmetric component ΔV_y^{anti} of the measured voltage as a function of magnetic field for different ΔT; it tracks one of the branches of a magnetization hysteresis loop. (b) Dependence of ΔV_{ISHE} on ΔT and linear fit. (c) Dependence of the Spin-Seebeck coefficient with the film thickness.

IV. CONCLUSIONS

We have demonstrated that monocrystalline YIG samples can be fabricated onto GGG (111) substrates through the water-based chemical route called polymer assisted deposition. Furthermore, film thickness control can be achieved with a single layer thickness resolution. XRD experiments and HRTEM images confirm the excellent crystallinity of the samples, and no interface can be perceived between the stacked layers.

The magnetic properties of the films grown by this technique are competitive with films grown by more standard PVD techniques, such as pulsed laser deposition. The coercive fields of the films are lower than 0.5 Oe and the 140 emu/cm^3 saturation magnetization value is close to that of bulk material. Ferromagnetic resonance experiments show a single sharp line with 6 G peak-to-peak amplitude, which is the smallest value achieved for a chemical route fabricated YIG sample. Damping value was extracted through two different methods obtaining similar results in the range of 10^{-3}, which is comparable to values reported in the literature.

The potential application of these samples in spintronic devices has been demonstrated with the spin-Seebeck effect measurements, exhibiting thermal-spin transformation in the range of nV K^{-1}.

In conclusion, PAD is a competitive and suitable technique for fabricating YIG thin films with precise thickness control, as demonstrated by the properties presented in this paper. Additionally, the water-based nature of the technique, makes it a highly versatile and cost-effective method, offering scalability for industrial applications in spintronics.

SUPPLEMENTARY MATERIAL

Additional information about the samples can be found in the supplementary material. There we present the x-ray diffraction pattern in the $20°$–$120°$ range, where only (hhh) peaks can be seen, confirming the full orientation of the crystal induced by the substrate. In addition, a detail of the (444) and (888) diffraction peaks of GGG and YIG is shown.

X-ray reflectivity profiles are included in the supplementary material and a table to summarize the properties of the samples obtained by the fitting of the data.

An AFM image of a 4×4 μm^2 section of a sample is shown, confirming the low rugosity in larger areas.

ACKNOWLEDGMENTS

AUTHOR DECLARATIONS

Conflict of Interest

The authors have no conflicts to disclose.

Author Contributions

Rubén Corcuera: Conceptualization (equal); Data curation (equal); Formal analysis (equal); Investigation (equal); Methodology (equal); Writing – original draft (equal). **Pilar Jiménez-Cavero**: Conceptualization (equal); Data curation (equal); Formal analysis (equal); Investigation (equal); Writing – original draft (equal). **Rafael Pérez del Real**: Data curation (equal); Formal analysis (equal); Investigation (equal). **Francisco Rivadulla**: Conceptualization (equal); Investigation (equal). **Rafael Ramos**: Data curation (equal); Investigation (equal). **José Ignacio Morales-Aragonés**: Data curation (equal); Formal analysis (equal); Investigation (equal). **Soraya Sangiao**: Data curation (equal); Formal analysis (equal); Investigation (equal). **César Magén**: Data curation (equal); Formal analysis (equal); Investigation (equal). **Luis Morellón**: Conceptualization (equal); Funding acquisition (equal); Investigation (equal); Project administration (equal); Supervision (equal). **Irene Lucas**: Conceptualization (equal); Data curation (equal); Formal analysis (equal); Funding acquisition (equal); Investigation (equal); Methodology (equal); Project administration (equal); Supervision (equal).

DATA AVAILABILITY

The data that support the findings of this study are available from the corresponding author upon reasonable request.

REFERENCES

[1] A. A. Serga, A. V. Chumak, and B. Hillebrands, J. Phys. D: Appl. Phys. **43**, 264002 (2010).

[2] J. Adam, L. Davis, G. Dionne, E. Schloemann, and S. Stitzer, IEEE Trans. Microwave Theory Tech. **50**, 721 (2002).

[3] B. J. H. Stadler and T. Mizumoto, IEEE Photonics J. **6**(1), 0600215 (2014).

[4] H. Wang, C. Du, P. Chris Hammel, and F. Yang, Appl. Phys. Lett. **104**, 202405 (2014).

[5] J. Barker and G. E. W. Bauer, Phys. Rev. Lett. **117**, 217201 (2016).

[6] N. S. Sokolov, V. V. Fedorov, A. M. Korovin, S. M. Suturin, D. A. Baranov, S. V. Gastev, B. B. Krichevtsov, K. Y. Maksimova, A. I. Grunin, V. E. Bursian, L. V. Lutsev, and M. Tabuchi, J. Appl. Phys. **119**, 023903 (2016).

[7] E. Mallmann, A. Sombra, J. Goes, and P. Fechine, Solid State Phenom. **202**, 65 (2013).

[8] R. C. LeCraw, E. G. Spencer, and C. S. Porter, Phys. Rev. **110**, 1311 (1958).

[9] S. Klingler, H. Maier-Flaig, C. Dubs, O. Surzhenko, R. Gross, H. Huebl, S. T. B. Goennenwein, and M. Weiler, Appl. Phys. Lett. **110**, 092409 (2017).

[10] H. Yu, O. d'Allivy Kelly, V. Cros, R. Bernard, P. Bortolotti, A. Anane, F. Brandl, R. Huber, I. Stasinopoulos, and D. Grundler, Sci. Rep. **4**, 6848 (2014).

[11] M. C. Onbasli, A. Kehlberger, D. H. Kim, G. Jakob, M. Kläui, A. V. Chumak, B. Hillebrands, and C. A. Ross, APL Mater. **2**, 106102 (2014).

[12] C. Hauser, T. Richter, N. Homonnay, C. Eisenschmidt, M. Qaid, H. Deniz, D. Hesse, M. Sawicki, S. G. Ebbinghaus, and G. Schmidt, Sci. Rep. **6**, 20827 (2016).

[13] S. Geller and M. Gilleo, J. Phys. Chem. Solids **3**, 30 (1957).

[14] E. E. Anderson, Phys. Rev. **134**, A1581 (1964).

[15] C. Dubs, O. Surzhenko, R. Linke, A. Danilewsky, U. Brückner, and J. Dellith, J. Phys. D: Appl. Phys. **50**, 204005 (2017).

[16] C. Dubs, O. Surzhenko, R. Thomas, J. Osten, T. Schneider, K. Lenz, J. Grenzer, R. Hübner, and E. Wendler, Phys. Rev. Mater. **4**, 024416 (2020).

09 September 2024 10:17:36

[17]N. Beaulieu, N. Kervarec, N. Thiery, O. Klein, V. Naletov, H. Hurdequint, G. de Loubens, J. B. Youssef, and N. Vukadinovic, IEEE Magn. Lett. **9**, 3706005 (2018).

[18]A. V. Chumak, P. Kabos, M. Wu, C. Abert, C. Adelmann, A. O. Adeyeye, J. Åkerman, F. G. Aliev, A. Anane, A. Awad, C. H. Back, A. Barman, G. E. W. Bauer, M. Becerer, E. N. Beginin, V. A. S. V. Bittencourt, Y. M. Blanter, P. Bortolotti, I. Boventer, D. A. Bozhko, S. A. Bunyaev, J. J. Carmiggelt, R. R. Cheenikundil, F. Ciubotaru, S. Cotofana, G. Csaba, O. V. Dobrovolskiy, C. Dubs, M. Elyasi, K. G. Fripp, H. Fulara, I. A. Golovchanskiy, C. Gonzalez-Ballestero, P. Graczyk, D. Grundler, P. Gruszecki, G. Gubbiotti, K. Guslienko, A. Haldar, S. Hamdioui, R. Hertel, B. Hillebrands, T. Hioki, A. Houshang, C.-M. Hu, H. Huebl, M. Huth, E. Iacocca, M. B. Jungfleisch, G. N. Kakazei, A. Khitun, R. Khymyn, T. Kikkawa, M. Kläui, O. Klein, J. W. Kłos, S. Knauer, S. Koraltan, M. Kostylev, M. Krawczyk, I. N. Krivorotov, V. V. Kruglyak, D. Lachance-Quirion, S. Ladak, R. Lebrun, Y. Li, M. Lindner, R. Macêdo, S. Mayr, G. A. Melkov, S. Mieszczak, Y. Nakamura, H. T. Nembach, A. A. Nikitin, S. A. Nikitov, V. Novosad, J. A. Otálora, Y. Otani, A. Papp, B. Pigeau, P. Pirro, W. Porod, F. Porrati, H. Qin, B. Rana, T. Reimann, F. Riente, O. Romero-Isart, A. Ross, A. V. Sadovnikov, A. R. Safin, E. Saitoh, G. Schmidt, H. Schultheiss, K. Schultheiss, A. A. Serga, S. Sharma, J. M. Shaw, D. Suess, O. Surzhenko, K. Szulc, T. Taniguchi, M. Urbánek, K. Usami, A. B. Ustinov, T. van der Sar, S. van Dijken, V. I. Vasyuchka, R. Verba, S. V. Kusminskiy, Q. Wang, M. Weides, M. Weiler, S. Wintz, S. P. Wolski, and X. Zhang, IEEE Trans. Magn. **58**, 0800172 (2022).

[19]S. Li, W. Zhang, J. Ding, J. E. Pearson, V. Novosad, and A. Hoffmann, Nanoscale **8**, 388 (2016).

[20]H. Chang, P. Li, W. Zhang, T. Liu, A. Hoffmann, L. Deng, and M. Wu, IEEE Magn. Lett. **5**, 6700104 (2014).

[21]S. Sangiao, J. Ignacio Morales-Aragones, I. Lucas, P. Jimenez-Cavero, L. Morellon, C. Sanchez-Azqueta, and J. M. De Teresa, J. Phys. D: Appl. Phys. **54**, 375305 (2021).

[22]R. Torrão, O. Alves, B. Archanjo, L. Sampaio, and F. Garcia, J. Alloys Compd. **923**, 166300 (2022).

[23]B. M. Howe, S. Emori, H.-M. Jeon, T. M. Oxholm, J. G. Jones, K. Mahalingam, Y. Zhuang, N. X. Sun, and G. J. Brown, IEEE Magn. Lett. **6**, 3500504 (2015).

[24]O. d'Allivy Kelly, A. Anane, R. Bernard, J. Ben Youssef, C. Hahn, A. H. Molpeceres, C. Carrétéro, E. Jacquet, C. Deranlot, P. Bortolotti, R. Lebourgeois, J.-C. Mage, G. de Loubens, O. Klein, V. Cros, and A. Fert, Appl. Phys. Lett. **103**, 082408 (2013).

[25]J. M. Vila-Fungueiriño, B. Rivas-Murias, B. Rodriguez-Gonzalez, O. Txoperena, D. Ciudad, L. E. Hueso, M. Lazzari, and F. Rivadulla, ACS Appl. Mater. Interfaces **7**, 5410 (2015).

[26]I. Lucas, P. Jiménez-Cavero, J. M. Vila-Fungueiriño, C. Magén, S. Sangiao, J. M. de Teresa, L. Morellón, and F. Rivadulla, Phys. Rev. Mater. **1**, 074407 (2017).

[27]A. Kehlberger, U. Ritzmann, D. Hinzke, E.-J. Guo, J. Cramer, G. Jakob, M. Onbasli, D. H. Kim, C. Ross, M. B. Jungfleisch, B. Hillebrands, U. Nowak, and M. Kläui, Phys. Rev. Lett. **115**, 096602 (2015).

[28]A. Anadón, R. Ramos, I. Lucas, P. A. Algarabel, L. Morellón, M. R. Ibarra, and M. H. Aguirre, Appl. Phys. Lett. **109**, 012404 (2016).

[29]A. Prakash, B. Flebus, J. Brangham, F. Yang, Y. Tserkovnyak, and J. P. Heremans, Phys. Rev. B **97**, 020408 (2018).

[30]G. E. W. Bauer, E. Saitoh, and B. J. van Wees, Nat. Mater. **11**, 391 (2012).

[31]S. M. Rezende, R. L. Rodríguez-Suárez, R. O. Cunha, A. R. Rodrigues, F. L. A. Machado, G. A. Fonseca Guerra, J. C. Lopez Ortiz, and A. Azevedo, Phys. Rev. B **89**, 014416 (2014).

[32]U. Ritzmann, D. Hinzke, and U. Nowak, Phys. Rev. B **89**, 024409 (2014).

[33]M. Althammer, J. Phys. D: Appl. Phys. **51**, 313001 (2018).

[34]E. Saitoh, M. Ueda, H. Miyajima, and G. Tatara, Appl. Phys. Lett. **88**, 182509 (2006).

[35]H. Adachi, K. Uchida, E. Saitoh, and S. Maekawa, Rep. Prog. Phys. **76**, 036501 (2013).

[36]T. J. Silva, C. S. Lee, T. M. Crawford, and C. T. Rogers, J. Appl. Phys. **85**, 7849 (1999).

[37]P. Cao Van, S. Surabhi, V. Dongquoc, R. Kuchi, S.-G. Yoon, and J.-R. Jeong, Appl. Surf. Sci. **435**, 377 (2018).

[38]M. Wu, "Nonlinear spin waves in magnetic film feedback rings," in *Solid State Physics*, 62 (Academic Press, 2010), pp. 163–224.

[39]J. Ding, T. Liu, H. Chang, and M. Wu, IEEE Magn. Lett. **11**, 1 (2020).

[40]C. Kittel, *Introduction to Solid State Physics*, 8th ed. (Wiley, 2004).

[41]E. Montoya, T. McKinnon, A. Zamani, E. Girt, and B. Heinrich, J. Magn. Magn. Mater. **356**, 12 (2014).

[42]M. B. Jungfleisch, A. V. Chumak, A. Kehlberger, V. Lauer, D. H. Kim, M. C. Onbasli, C. A. Ross, M. Kläui, and B. Hillebrands, Phys. Rev. B **91**, 134407 (2015).

[43]D. Stancil and A. Prabhakar, *Spin Waves: Theory and Applications* (Springer US, 2009).

[44]J. P. Nibarger, R. Lopusnik, and T. J. Silva, Appl. Phys. Lett. **82**, 2112 (2003).

[45]T. Kikkawa, K. Uchida, Y. Shiomi, Z. Qiu, D. Hou, D. Tian, H. Nakayama, X.-F. Jin, and E. Saitoh, Phys. Rev. Lett. **110**, 067207 (2013).

[46]A. Sola, V. Basso, M. Kuepferling, C. Dubs, and M. Pasquale, Sci. Rep. **9**, 2047 (2019).

[47]H. Nakayama, K. Ando, K. Harii, T. Yoshino, R. Takahashi, Y. Kajiwara, K. Uchida, Y. Fujikawa, and E. Saitoh, Phys. Rev. B **85**, 144408 (2012).

09 September 2024 10:17:36